CHAPTER 7

POOL BOILING HEAT TRANSFER OF FC-72 ON ARTIFICIAL MICRO-CAVITY SURFACES

Silicon is widely used in many VLSI electron devices but the studies on understanding the mechanism of pool boiling from micro structure on silicon base surfaces are still limited. In this chapter, artificial micro-cavity surfaces with different geometric parameters and orientations are tested in order to investigate the pool boiling characteristics. The test surfaces are manufactured on a 10mm×10mm square silicon plate. The treated cavities with cylindrical shape have three different diameters of 200, 100 and 50μm and two different depths of 200 and 110μm. The arrangements of the cavities are designed to be 33×33, 25×25 and 16×16 array. Base on the present measured data, the characteristics of heat transfer for pool boiling of FC-72 on artificial micro-cavity surfaces are examined. Moreover, visualization of the flow patterns is conducted in order to investigate the characteristics of the bubbles in growth and departure processes. The effects of heat flux, cavity density, cavity diameter, and orientations on pool boiling heat transfer coefficient and bubble characteristics are inspected in details.

7.1 Flow Pattern Observation of Micro-Cavity Surfaces

To illustrate the characteristics of saturated FC-72 boiling on micro-cavity surfaces, photographs with different cavity densities and orientations are shown in Figure 7.1, 7.2 and 7.3. A closed inspection of the photographs in Figure 7.1 (a), 7.2 (a) and 7.3 (a) indicate that at boiling incipience the bubble population is sparse but uniformly and randomly distributes over the cavities. Bubble birth and bubble departure seem to be periodic, and shapes of bubbles are almost perfectly spherical. Besides, the observed bubbles departing from cavities are small and discrete without any interaction or coalescence. For a little raise in the heat flux values, as shown in Figure 7.1(b), 7.2 (b) and 7.3(b), both the number of active cavities and bubble departure frequency increase. Higher bubble departure frequency also induces vertical

coalescence above some cavities after the bubbles leave the cavities. At moderate heat flux, as shown in Figure 7.1 (c), 7.2 (c) and 7.3 (c), some growing bubbles begin to coalesce horizontally with each other on adjacent cavities so that the cavity surface is covered with coalesced bubbles and some vapor columns are formed. Obviously, coalesced bubbles contribute flow resistance to obstruct the re-wetting liquid from entering the cavities and also to delay the bubbles departure at the same time. Finally, at high heat flux region as shown in Figure 7.1(d), 7.2 (d) and 7.3 (d), it is clearly observed that large vapor mushroom clouds blanket the entire cavity surface. As the heat flux approaches to CHF, the vapor mushroom cloud becomes a twisted column filled with large bubbles. Apparently, this twisted column cause exhaustion of re-wetting liquid and result in the dry-out situation near the central portion of the test surface.

7.2 The Effects of the Cavity Density on Boiling Heat Transfer Performance

The heat flux plotted against the wall superheat for both single-phase natural convection and nucleate boiling regime on three cavity surfaces with different cavity densities is showed in Figure 7.4. During the natural convection regime, it is note that only slightly difference in wall superheat with the cavity density. For all test surfaces, the significant temperature excursion is observed as the bubbles are generated. The wall superheat decreases suddenly because the bubble absorbs a large amount of heat as the dielectric liquid boils in the cavities. In addition, a extremely high incipience superheat of plain silicon surface of 45.9K is observed because of least nucleate sites on its highly polished surface. By contrast, the reduction of boiling incipience superheat and temperature excursions of micro-cavity surfaces are also seen in Figure 7.4. In the nucleate boiling regime, the wall superheat of the cavity surface is significantly lower than that of the plain surface due to more nucleate sites on the micro-cavity surface. The results indicate that the pool boiling performance of micro-cavity surface is better than that of the plain surface at the same heat flux. The boiling curve shifts to left with denser

cavity surface showing better pool boiling enhancement. The plots in Figure 7.4 also show that a noticeable enhancement in CHF value of all micro-cavity surfaces is due to the increase in nucleate sites. For the 33×33 array surface, the CHF value of 30 W cm^{-2} is almost 2.5 times that of the plain silicon surface.

The heat transfer coefficient of the test surfaces is plotted versus heat flux in Figure 7.5. The heat transfer coefficient of the test surfaces shows the same trend with heat flux. As the heat flux increases, the heat transfer coefficients reach a maximum value and then declines. The peak is at about 1.8×10^{5} W m^{-2} for 16×16 arrangement and 25×25 arrangement cavity array surfaces and 1.2×10^{5} W m^{-2} for 33×33 arrangement cavity array surface. This maximum value can be explained by the fact that the active nucleate density increases as the wall temperature rises until large clusters and accumulations of bubble are formed near the heating surface. After this peak value, the heat transfer coefficients begin to drop. This behavior is induced by two types of liquid/vapor exchange mechanism: temporal dry-out situation inside the cylindrical cavities and vapor film blanket the heating surface. Temporal dry-out situation is the result of the flow resistance in cavity structure with vapor trapped inside which impedes re-wetting fluid flow into the cavity. Moreover, vapor coalescences among the adjacent cavities form the vapor film to cover the heating surface as a larger of thermal insulation.

The effects of density of cavities on CHF value variations for six test surfaces are shown in Figure 7.6. The micro-cavity surfaces consistently enhance the CHF value over the plain silicon surface. However, this enhancement mechanism seems to reach a critical value with denser cavity array. This implies that the CHF values cannot always be raised with increasing the of cavity density.

7.3 Effects of Cavity Diameter and Depth on Boiling Heat Transfer Coefficient

The boiling performances of the micro-cavity surfaces with various cavity diameters of 50, 100 and 200μm are plotted in Figure 7.7. The cavity density is of 25×25 array, with 110μm

depth. Figure 7.7 shows the slopes of the boiling curves are roughly the same regardless of the cavity diameter in the low heat flux region. This indicates that the influence of the cavity diameter on heat transfer coefficients can be ignored in the low heat flux region below 8×10^4 W m^{-2}. The same trends are also observed by Shoji et al. [44]. However, earlier decay and lower peak value of boiling heat transfer coefficient for larger cavity diameter surface are observed in the moderate and high heat flux regions. The reason is that the departure bubble diameter increases with cavity diameter and the growing bubbles from larger diameter cavity can easily coalesce with adjacent bubbles due to smaller cavity spacing. This bubble interaction manifests that horizontal coalescence of bubbles in the moderate and high heat flux regions.

Next, the effects of the cavity depth on overall boiling heat transfer coefficient are also examined in Figure 7.8. The figure presents the behaviors of the overall heat transfer coefficients on micro-cavity surfaces with cavity densities of 33×33 and 16×16 and cavity depth of 200 and 110μm. Note that the premature rapid decline of the overall heat transfer coefficients for deeper cavity surfaces. In the nucleate boiling region, the hydrodynamic interaction of the vapor/liquid exchange mechanism can be influenced by the cavity depth. Deeper cavities trap the departure bubbles and reduce the bubble departure frequency. Then the trapped bubble leaves the residual vapor to remain inside the cavities which in turn form the flow resistance to obstruct the re-wetting liquid from entering the cavities.

7.4 Effect of Orientation on Pool Boiling Heat Transfer Coefficient

Finally, the overall heat transfer coefficients of cavity surfaces versus heat flux for two cavity density 33×33 and 16×16 at both horizontal and vertical orientations are shown in Figure 7.9. The results indicate that the pool boiling heat transfer coefficients of vertical surface are higher than those of the horizontal counterpart prior to the peak value. This trend is more prominent for denser cavity surface which is attributed to the fact that bubbles are trapped inside the cavities and the vertical coalescence of bubbles drifts along vertical surface.

It is further noted that vertical cavity surface has lower heat transfer coefficients beyond the peak value due to the fact that thick vapor mushrooms blanket the entire vertical cavity surface and form a larger thermal resistance.

7.5 Conclusion Remarks

This chapter reports an experimental study on the saturated pool boiling of FC-72 on different artificial micro-cavity surfaces. The pool boiling heat transfer performances and flow patterns of these cavity surfaces are also discussed. The major results obtained can be briefly summarized in the following:

1. The boiling incipience superheat and temperature excursion on silicon-base surfaces are more significant than that on metal based surfaces.
2. For horizontal micro-cavity surfaces, the overall heat transfer coefficient decreases as the cavity density increases. Moreover, the effect of cavity density is stronger at high heat flux region than that in low heat flux region because of the horizontal bubble/vapor coalescence near the heating surface. Besides, the CHF values are raised with the cavity density and area enhancement of the cavities surface.
3. The influence of the cavity diameter in heat transfer coefficients during the low heat flux region below 8×10^{4} W m^{-2} can be ignored. In moderate and high heat flux regions, larger cavity diameter surface show earlier decay and lower peak value in the pool boiling heat transfer coefficient.
4. Increasing the depth of cavities will result early rapid decline of overall heat transfer coefficient due to the larger flow resistance inside the deeper cavities and obstruction of the re-wetting liquid entering the those cavities.
5. The maximum value of CHF is 3×10^{5} W cm^{-2} for the horizontal test surface with 33×33 cavity array, which is almost 2.5 times of plain silicon surface
6. Comparison between boiling between the horizontal and vertical orientations on

micro-cavity surfaces shows a significant decrease in overall heat transfer coefficient in high heat flux region for the vertical orientation due to the vapor coalescence along the heating surface and dry-out situation inside the cavity on the vertical heating surface.

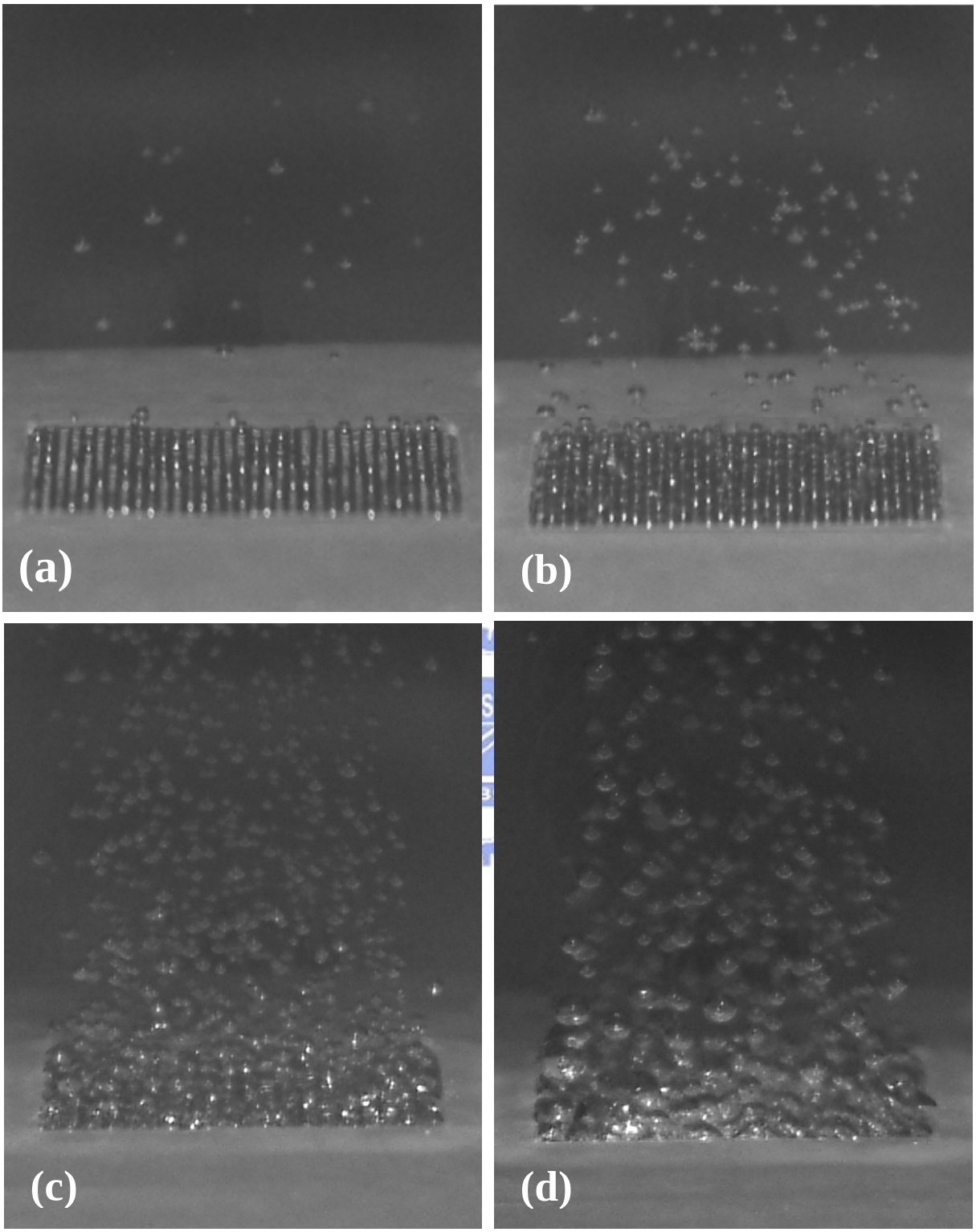

Figure 7.1 Flow patterns of micro-cavity surface with cavity density of 33×33 array in horizontal orientation: (a) 11.5% of CHF; (b) 26.3% of CHF; (c) 62.8% of CHF; (d) 80.1% of CHF.

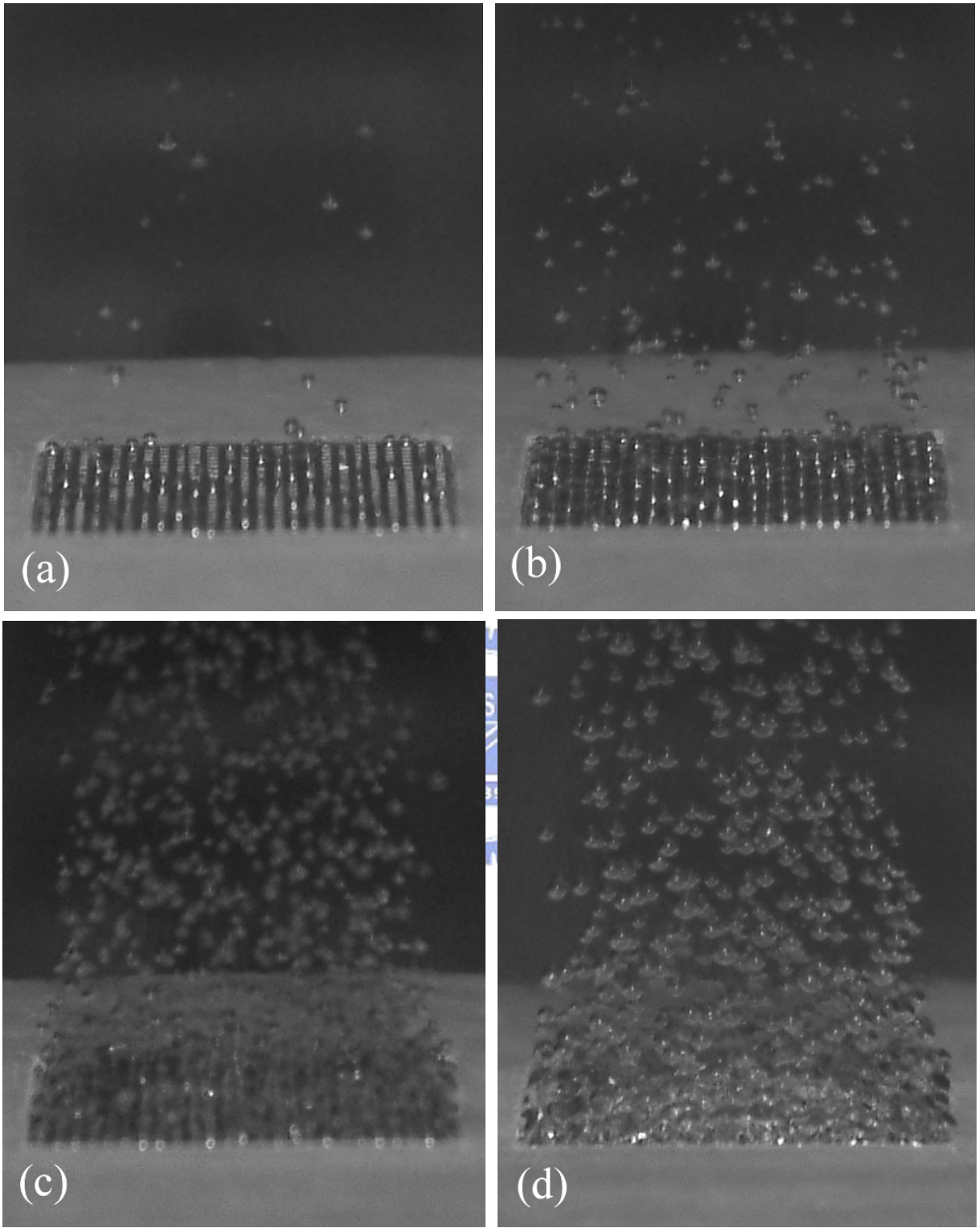

Figure 7.2 Flow patterns of micro-cavity surface with cavity density of 25×25 array in horizontal orientation: (a) 11.7% of CHF; (b) 28.4% of CHF; (c) 56.5% of CHF; (d) 78.6% of CHF.

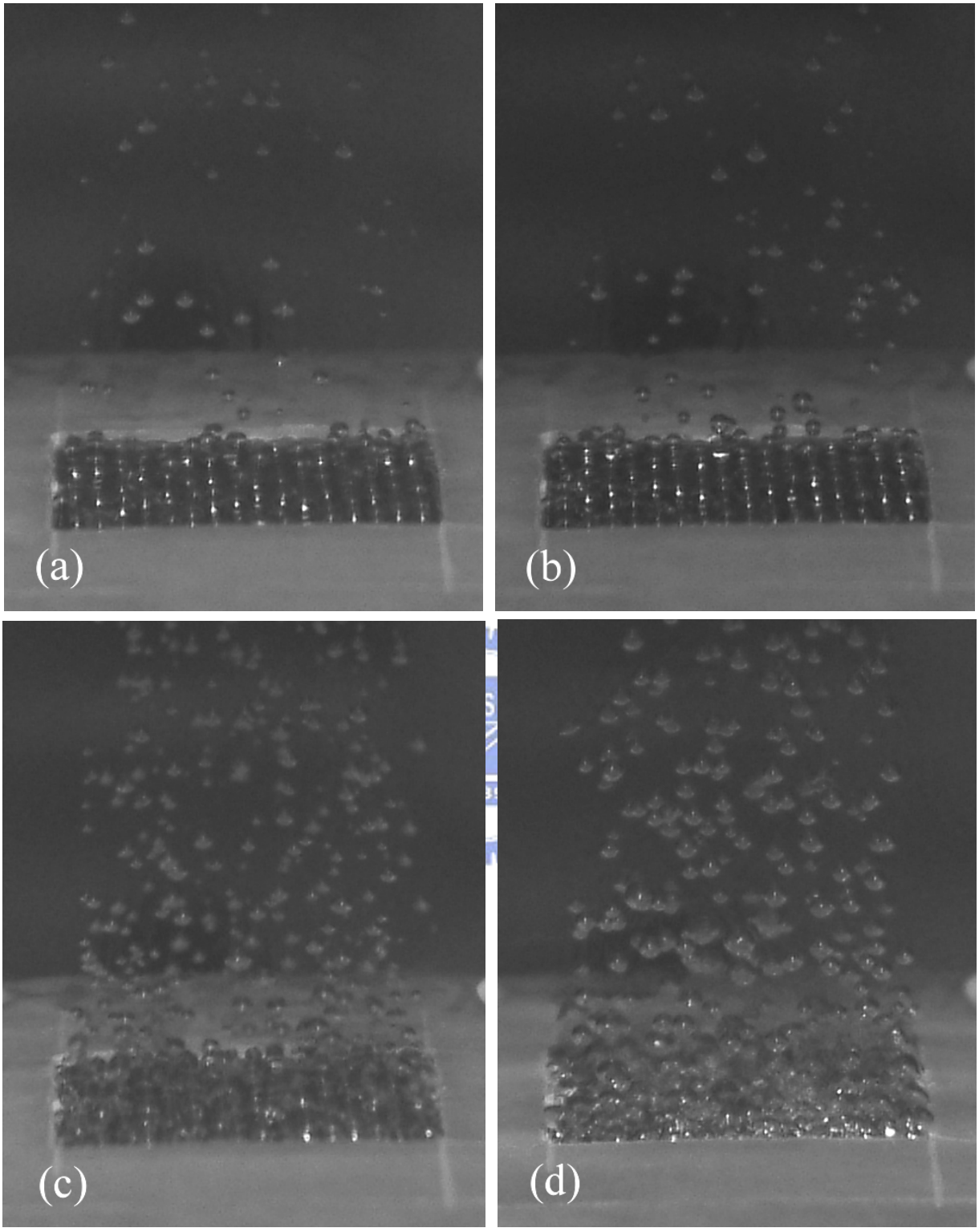

Figure 7.3 Flow patterns of micro-cavity surface with cavity density of 16×16 array in horizontal orientation: (a) 14.8% of CHF; (b) 33.9% of CHF; (c) 55.1% of CHF; (d) 75.9% of CHF.

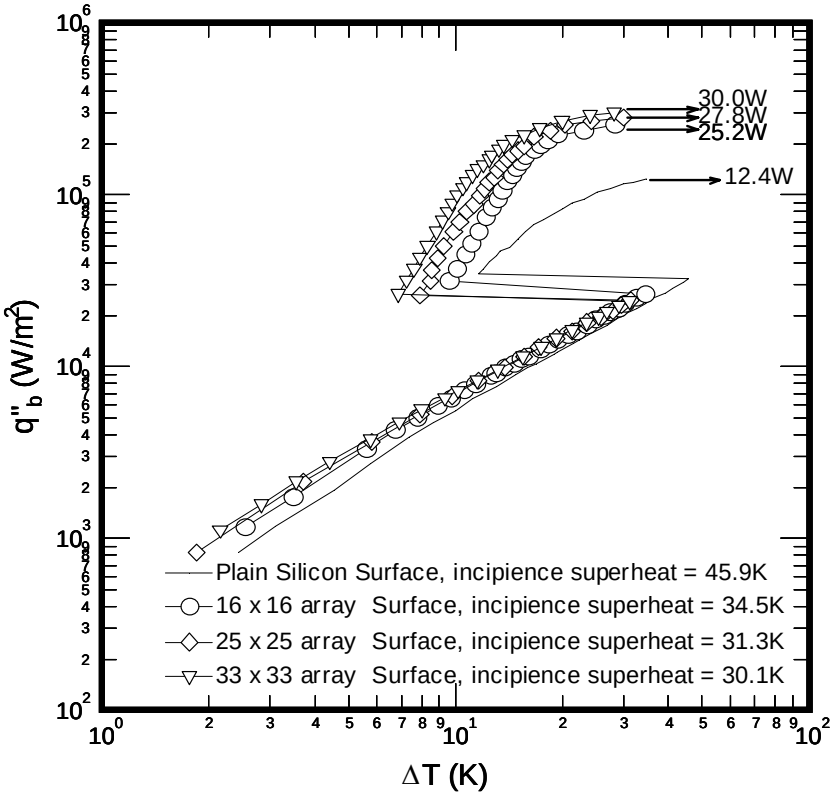

Figure 7.4 Boiling curves of micro-cavity surface in horizontal orientation (cavity diameter 200μm, depth 110μm).

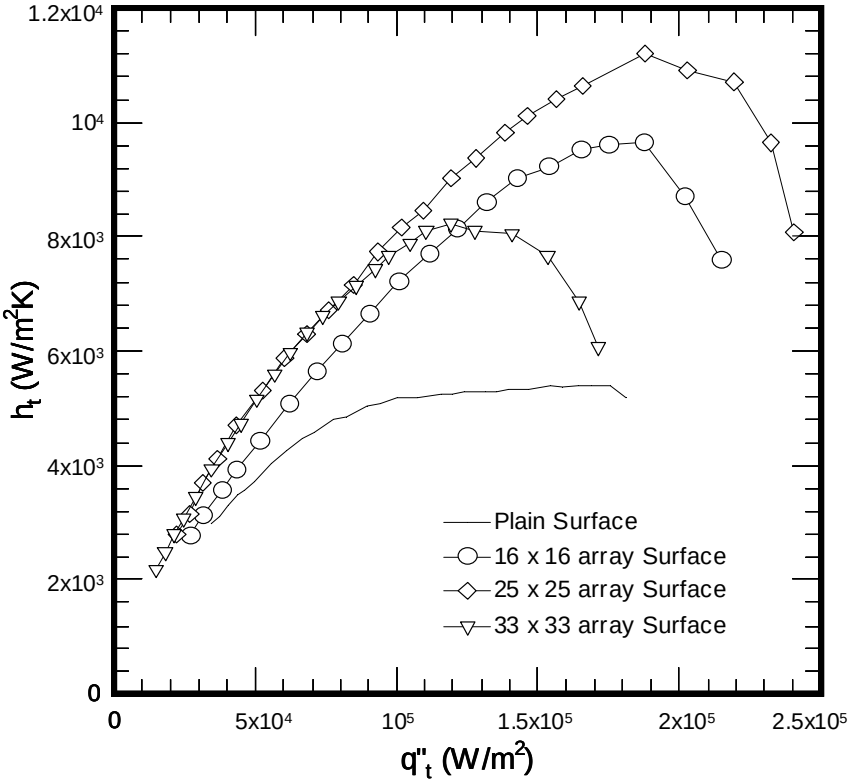

Figure 7.5 Variations of pool boiling heat transfer coefficient with heat flux for various cavity density surfaces in horizontal orientation (Decreasing heat flux).

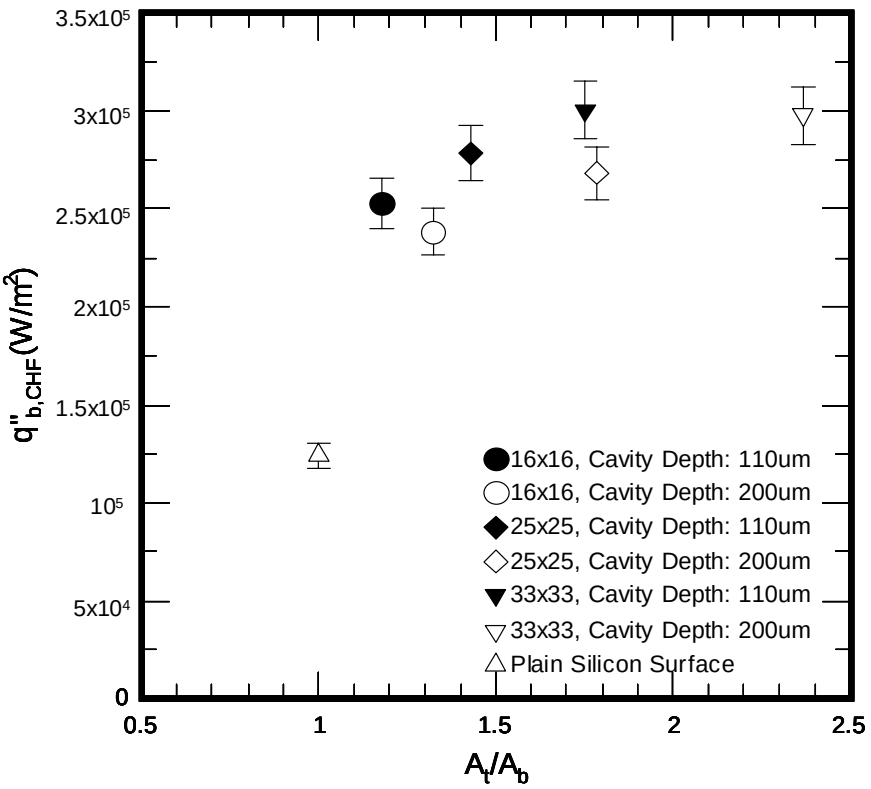

Figure 7.6 Variations of critical heat flux with enhancement of area at two cavity depths 110 and 200μm (horizontal orientation).

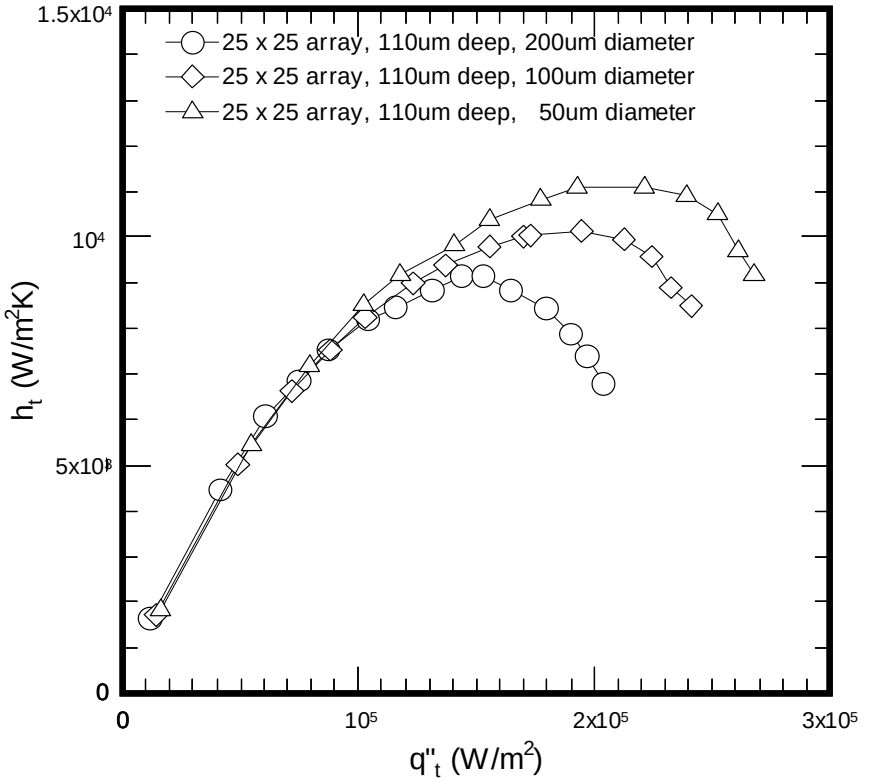

Figure 7.7 Variations of pool boiling heat transfer coefficient with heat flux for various cavity diameters in horizontal orientation (Decreasing heat flux).

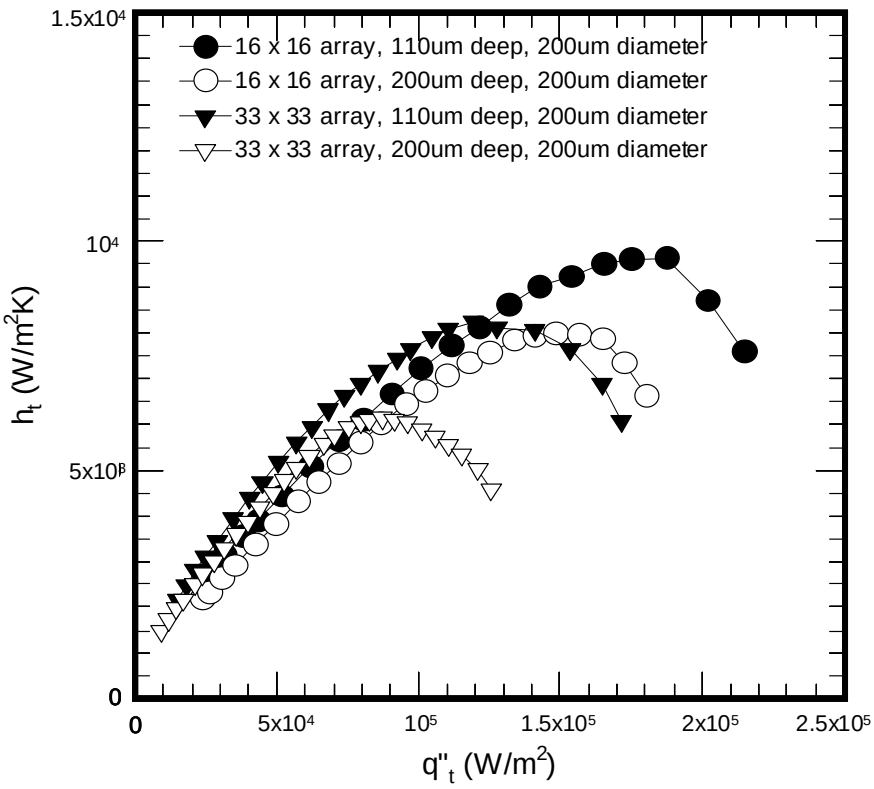

Figure 7.8 Variations of pool boiling heat transfer coefficient with heat flux for various cavity depths in horizontal orientation (Decreasing heat flux).

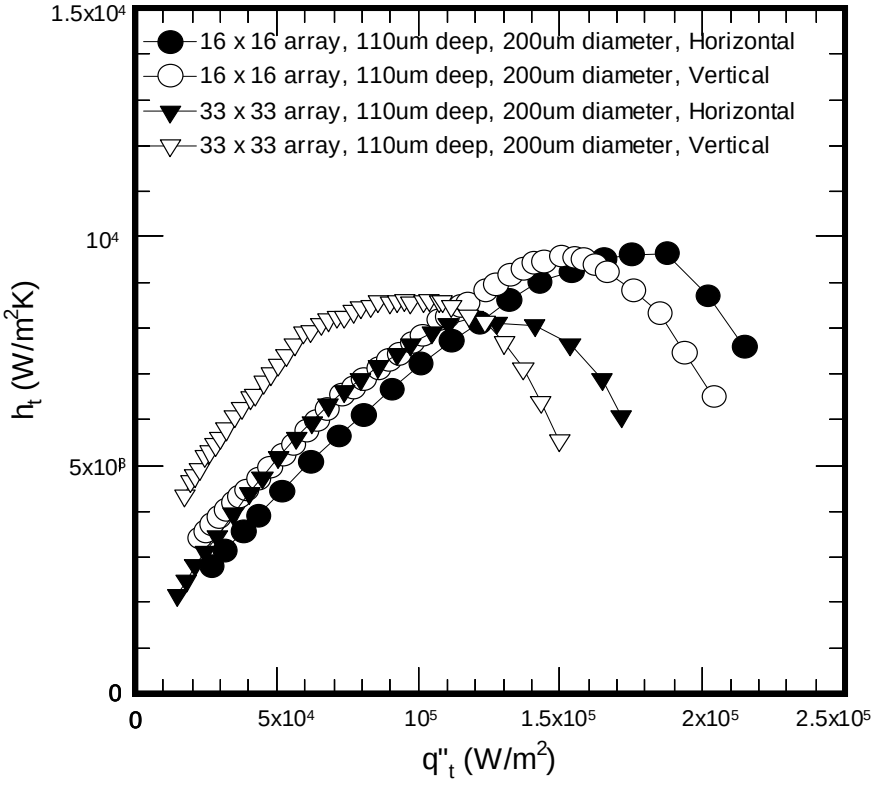

Figure 7.9 Variations of pool boiling heat transfer coefficient with heat flux at horizontal and vertical orientation (Decreasing heat flux).